Acta Crystallographica Section B
Structural Science
ISSN 0108-7681

Structures of three dehydration products of bischofite from *in situ* synchrotron powder diffraction data ($MgCl_2 \cdot nH_2O$; n = 1, 2, 4)

Kunihisa Sugimoto,[a] Robert E. Dinnebier[a]* and Jonathan C. Hanson[b]

[a]Max-Planck Institute for Solid State Research, Heisenbergstrasse 1, D-70569 Stuttgart, Germany, and [b]Chemistry Department, Brookhaven National Laboratory, Upton, NY 11973, USA

Correspondence e-mail: r.dinnebier@fkf.mpg.de

Received 2 November 2006
Accepted 17 January 2007

High-quality *in situ* synchrotron powder diffraction data have been used to investigate the decomposition products of bischofite in the temperature range $298 \leq T \leq 873$ K. At least eight phases could be identified: $MgCl_2 \cdot nH_2O$ (n = 1, 2, 4 and 6), $MgOHCl \cdot nH_2O$ ($0 \leq n \leq 1.0$), $MgCl_2$ and MgO. The crystal structures of three magnesium chloride hydrates $MgCl_2 \cdot nH_2O$ (n = 1, 2, 4) were determined *ab initio*, replacing published Rietveld refinements from low-quality powder diffraction data based on similarity criteria. $MgCl_2 \cdot 4H_2O$ was found to be disordered and has been correctly determined for the first time. The crystal structures of bischofite and $MgCl_2 \cdot 4H_2O$ consist of discrete $Mg(H_2O)_6$ and $MgCl_2(H_2O)_4$ octahedra, respectively. The crystal structure of $MgCl_2 \cdot 2H_2O$ is formed by single chains of edge-sharing $MgCl_2(H_2O)_4$ octahedra, while in the case of $MgCl_2 \cdot H_2O$ double chains of edge-sharing $MgCl(H_2O)_5$ octahedra are found. The phases in the system $MgCl_2$–H_2O are intermediates in the technologically important process of MgO and subsequently Mg production. The same phases were recently found to be of key importance in the understanding of cracks in certain magnesia concrete floors.

1. Introduction

The mineral bischofite, $MgCl_2 \cdot 6H_2O$ (Fig. 1), is a crystalline marine evaporate which was named after the German chemist Karl Gustav Bischof (1792–1870), who was the first to discover it in 1876 between rock salt layers in Leopoldshall near Stassurt. Bischofite, which is very hygroscopic, has a characteristic bitter-salty, pungent, burning taste. It is widely distributed and quite common in formations with different geologic ages.

Bischofite has a huge variety of applications in industry and medicine. Most importantly it is a raw material for the production of magnesium oxide, magnesium hydroxide and magnesium metal. From 1 m^3 of bischofite brine with a density of 420 kg m^{-3}, 177 kg of magnesium oxide or 107 kg of magnesium metal can be produced. Bischofite itself is an effective and fast ice melter, acts as a versatile fertilizer, is used in fire protection and fire fighting, and has various medical applications as a basis for a series of drugs.

Bischofite crystallizes in the monoclinic space group *C2/m* with lattice parameters of a = 9.8607 (2), b = 7.1071 (2), c = 6.0737 (2) Å, β = 93.758 (2)°, Z = 2. Its crystal structure was first determined in 1934 by Andress & Gundermann (1934).

During our investigation of the thermal decomposition of chlorartinite (Sugimoto *et al.*, 2006), a volcanic exhalation product also found in some magnesia concrete floors, several phases of magnesium chloride hydrate including bischofite were encountered, most of which do not have a reported or

confirmed crystal structure. The only source for structural information was a paper by Kaduk (2002), where the crystal structures of $MgCl_2{\cdot}nH_2O$ ($n = 1, 2, 4$) were anticipated on the basis of comparison to similar compounds in the ICSD database and later refined using low-quality X-ray powder diffraction data from poorly diffracting samples isolated from preparations of polypropylene catalysts.

A variety of papers have been published on the thermal decomposition and reaction kinetics of bischofite and its subsequent dehydrated phases (Kashani-Nejad *et al.*, 2005; Galwey & Laverty, 1989; Kirsh *et al.*, 1987; Gardner & Messing, 1984; Herbstein *et al.*, 1982; Petzold & Naumann, 1980; Buzagh-Gere *et al.*, 1973). They all agree that heating rate as well as pressure and composition of the surrounding atmosphere strongly influence the transition temperatures and the occurrence of the different alkaline magnesium chlorides. In particular, the phase $MgOHCl{\cdot}nH_2O$ ($0.0 \leq n \leq 1.0$) is a subject of controversial discussion concerning the amount of water in the crystal structure. Unfortunately, the low crystallinity and therefore the low quality of the powder pattern of MgOHCl does not permit the determination of the crystal structure.

Due to the technological importance of the system $MgCl_2$–H_2O and the lack of structural information, we decided to investigate the thermal decomposition of bischofite up to a temperature of $T = 873$ K by the method of *in situ* synchrotron powder diffraction and to accurately determine the crystal structures of all insufficiently characterized crystalline phases which occur in the course of the dehydration process.

2. Experimental

2.1. Preparation

$MgCl_2{\cdot}6H_2O$ (bischofite) from Aldrich Chemical Co was used as purchased.

2.2. Thermal analyisis

Thermal analysis of bischofite was conducted using simultaneous DTA/TGA/MS techniques. For DTA/TGA/MS investigations a simultaneous thermal analyzer STA 409 (Netzsch, Selb) was used with the samples in alumina crucibles in an argon gas (99.999%) flow of 100 ml min^{-1} at a heating rate of 5 K min^{-1} (Fig. 2).

2.3. Powder diffraction

In situ powder diffraction data were collected at the SUNY X7B beamline at the National Synchrotron Light Source, Brookhaven National Laboratory. X-rays of wavelength $\lambda = 0.92187$ Å were selected by a double flat-crystal monochromator in an ultra-high vacuum located 8 m from the source. The X-ray beam was focused vertically by a spherical rhodium-coated silicon carbide mirror located 5 m from the source and horizontally by a cylindrical aluminium mirror with nickel plating coated by rhodium located 13 m from the source. The size of the beam was adjusted to a height of approximately 0.5 mm and a width of 2 mm. As the detector a MAR 345 image plate reader was set up perpendicular to the beam path at a distance of approximately 140 mm from the sample. LaB_6 (SRM660a) was used as an external standard to determine the beam center, sample-to-detector distance, exact wavelength and tilting angle of the image plate. The sample was contained in one-side-opened quartz capillaries with diameter 0.5 mm loaded in a sapphire tube of 0.8 mm diameter attached to a flow-reaction cell (Parise *et al.*, 2000; Chupas *et al.*, 2001). The temperature was monitored and controlled by a 0.01 in K thermocouple (Omega), which was inserted straight into the sapphire tube adjacent to and contacting the sample capillary. The sample was aligned such that the sample closest to the thermocouple was in the X-ray beam path. The flow cell was purged by helium gas (99.999%) and the exit gases were analyzed by an SRS rare-gas analyzer. The sample was heated

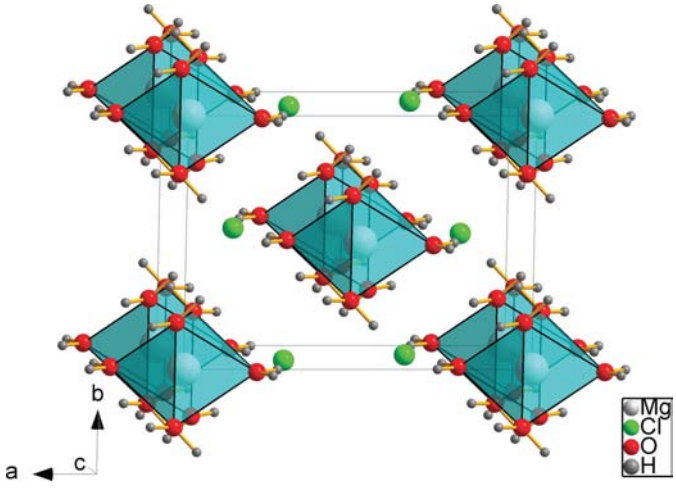

Figure 1
The crystal packing of $MgCl_2{\cdot}6H_2O$ (bischofite; Andress & Gundermann, 1934) in a parallel projection approximately down the crystallographic *c* axis. Mg-atom positions are in white, Cl-atom positions are in green, O-atom positions are in red and H-atom position are in gray.

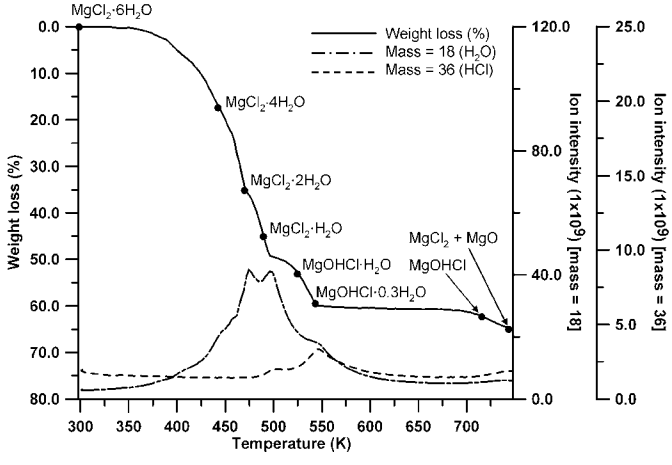

Figure 2
Thermogravimetric analysis (TGA) and mass spectrometry of mass number 18 (H_2O) and 36 (HCl) for bischofite, $MgCl_2{\cdot}6H_2O$, on heating up from 298 to 773 K. Points of weight loss (%) were estimated from molecular weight based on the formula.

Table 1
Experimental details.

	$MgCl_2{\cdot}4H_2O$	$MgCl_2{\cdot}2H_2O$	$MgCl_2{\cdot}H_2O$
Crystal data			
Chemical formula	$Cl_2H_8MgO_4$	$Cl_2H_4MgO_2$	Cl_2H_2MgO
M_r	167.27	131.24	113.23
Cell setting, space group	Orthorhombic, *Cmcm*	Monoclinic, *C*2/*m*	Orthorhombic, *Pnma*
Temperature (K)	358	369	434
a, *b*, *c* (Å)	4.21616 (13), 11.0230 (4), 7.2951 (3)	7.4279 (4), 8.5736 (4), 3.65065 (16)	8.9171 (6), 3.63421 (18), 11.4775 (7)
β (°)	90.0	98.580 (2)	90.0
V (Å^3)	339.04 (2)	229.89 (2)	371.95 (4)
Z	2	2	4
D_x (Mg m^{-3})	1.638	1.896	2.022
Radiation type	Synchrotron	Synchrotron	Synchrotron
Specimen form, colour	Particle morphlogy, white	Particle morphlogy, white	Particle morphlogy, white
Data collection			
Diffractometer	NSLS X7B	NSLS X7B	NSLS X7B
Data collection method	Specimen mounting: quartz capillary; mode: transmission	Specimen mounting: quartz capillary; mode: transmission	Specimen mounting: quartz capillary; mode: transmission
2θ (°)	$2\theta_{min}$ = 5.308, $2\theta_{max}$ = 49.415, increment = 0.0218	$2\theta_{min}$ = 5.308, $2\theta_{max}$ = 49.415, increment = 0.0218	$2\theta_{min}$ = 5.308, $2\theta_{max}$ = 49.415, increment = 0.0218
Refinement			
Refinement on	Full-matrix least-squares on F^2	–	–
R factors	R_p = 0.011, R_{wp} = 0.019, R_{exp} = 0.036	R_p = 0.010, R_{wp} = 0.017, R_{exp} = 0.036	R_p = 0.009, R_{wp} = 0.012, R_{exp} = 0.037
Wavelength of incident radiation (Å)	0.92187	–	–
Profile function	CW profile function No. 4 with 18 terms	CW profile function No. 4 with 18 terms	CW profile function No. 4 with 18 terms
No. of parameters	12	10	17
H-atom treatment	H-atom parameters not defined	Refined independently	Refined independently
Weighting scheme	LOOPARRAY	LOOPARRAY	LOOPARRAY
$(\Delta/\sigma)_{max}$	<0.0001	<0.0001	<0.0001

in the temperature range 298–873 K with a small resistance heater wrapped around the sapphire tube. The heating rate was 3.33 K min^{-1}. During exposure, the sample was rocked for several degrees in order to improve randomization of the crystallites. An exposure time of 30 s was chosen based on the saturation intensity of the image plate. The total time per scan was 110 s arising from the read-out time of 80 s. Integration of the full-circle powder patterns was performed using the program *POWDER*3*D* (Hinrichsen *et al.*, 2006) resulting in diagrams of corrected intensities *versus* the scattering angle 2θ (Fig. 3) in steps of 0.0218° (2θ) from 5.308° to 49.416° (2θ). Spikes owing to the large grain sizes of highly crystalline bischofite and reflections owing to the single-crystal sapphire capillary were automatically excluded by *POWDER*3*D*. After

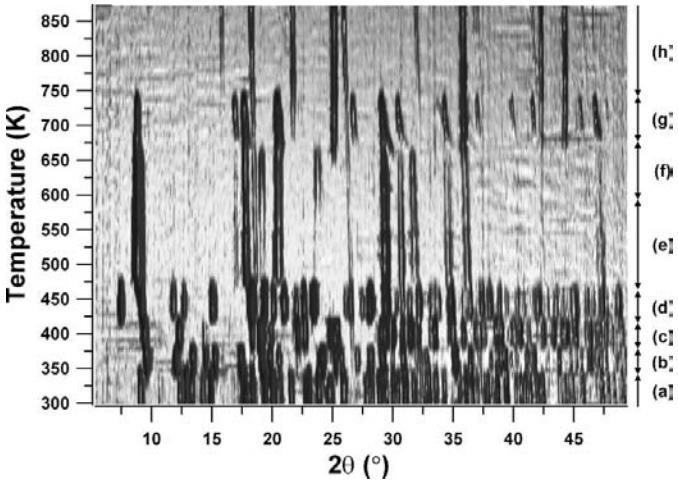

Figure 3
Two-dimensional projection (simulated heating-Guinier pattern) of the observed scattered X-ray intensity for magnesium chloride hydrate as a function of diffraction angle (x axis, 6.0−48.0° 2θ) and temperature (y axis, 298–873 K, 3.33 K min^{-1}, scans 1–94). The wavelength was 0.92187 Å. The observed phases were identified as follows; (*a*) $MgCl_2{\cdot}6H_2O$; (*b*) $MgCl_2{\cdot}4H_2O$; (*c*) $MgCl_2{\cdot}2H_2O$; (*d*) $MgCl_2{\cdot}H_2O$; (*e*) and (*f*) $MgOHCl{\cdot}nH_2O$, $0.0 \leq x \leq 1.0$; (*g*) $MgCl_2$–MgO; (*h*) MgO. This figure was prepared with *POWDER*3*D* (Hinrichsen *et al.*, 2006).

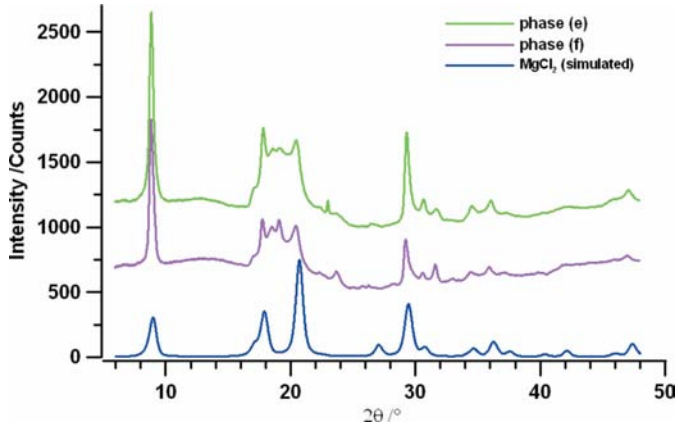

Figure 4
Scattered X-ray intensity for phase (*e*) at T = 542 K and (*f*) at T = 640 K for $MgOHCl{\cdot}nH_2O$, $0.0 \leq x \leq 1.0$, and $MgCl_2$ (simulated) as a function of diffraction angle 2θ. The wavelength was λ = 0.92187 Å. The simulated powder pattern of $MgCl_2$ was calculated using *FullProf* with ICSD database 86439 (Partin & O'Keeffe, 1991).

Table 2
Reaction schemes for thermal decomposition of bischofite, $MgCl_2{\cdot}6H_2O$, with transition temperatures as derived from *in situ* synchrotron powder pattern data recorded in a dry helium gas stream.

Phase	Equation	Transition temperature (K)
(*a*)	$MgCl_2{\cdot}6H_2O$	298
(*b*)	$MgCl_2{\cdot}6H_2O \rightarrow MgCl_2{\cdot}4H_2O + 2H_2O$	369
(*c*)	$MgCl_2{\cdot}4H_2O \rightarrow MgCl_2{\cdot}2H_2O + 2H_2O$	380
(*d*)	$MgCl_2{\cdot}2H_2O \rightarrow MgCl_2{\cdot}H_2O + H_2O$	426
(*e*)	$MgCl_2{\cdot}H_2O \rightarrow Mg(OH)Cl{\cdot}nH_2O + HCl + (1-n)\,H_2O$ $(0 \leq n \leq 0.3)$	466
(*f*)	$Mg(OH)Cl{\cdot}0.3H_2O \rightarrow Mg(OH)Cl + 0.3H_2O$	612
(*g*)	$2Mg(OH)Cl \rightarrow MgO + MgCl_2 + H_2O$	671
(*h*)	$MgCl_2 + H_2O \rightarrow MgO + 2HCl$	741

the first step of dehydration, the diffracted intensity of all the observed phases was quite uniformly distributed over the Debye–Scherrer rings, ruling out severe grain-size effects and preferred orientation. $MgCl_2{\cdot}4H_2O$ was the most crystalline phase of all lower hydrates of magnesium chloride with low-angle diffraction peaks having a minimum FWHM of 0.215° (2θ).

3. Structure solution and refinement

A two-dimensional projection (simulated heating-Guinier patterns) of the observed scattered X-ray intensities for magnesium chloride hydrate as a function of temperature is shown in Fig. 3. At least eight different phase ranges could be identified, partly using the program *Match* (Brandenburg & Putz, 2006): (*a*) $MgCl_2{\cdot}6H_2O$, (*b*) $MgCl_2{\cdot}4H_2O$, (*c*) $MgCl_2{\cdot}2H_2O$, (*d*) $MgCl_2{\cdot}H_2O$, (*e*) and (*f*) $MgOHCl{\cdot}nH_2O$ $(0.0 \leq n \leq 1.0)$, (*g*) $MgCl_2$ and MgO, and (*h*) MgO.

The crystal structures of $MgCl_2{\cdot}6H_2O$, $MgCl_2$ and MgO were taken from the ICSD database (Agron & Busing, 1985; Partin & O'Keeffe, 1991; Chizmeshya *et al.*, 2002). Any attempts to determine the crystal structures of $MgOHCl{\cdot}nH_2O$ $(0 \leq n \leq 1.0)$ did not succeed because of the low crystallinity of the compounds (Fig. 4). For the structure determination of $MgCl_2{\cdot}nH_2O$ (n = 1, 2, 4), the powder patterns at T = 358 K (scan No. 12) for $MgCl_2{\cdot}4H_2O$, at T = 396 K (scan No. 19) for $MgCl_2{\cdot}2H_2O$, at T = 434 K (scan No. 26) for $MgCl_2{\cdot}H_2O$, at T = 542 K (scan No. 41), and at T = 640 K (scan No. 57) were selected (Figs. 5–7). Indexing and space-group determination of $MgCl_2{\cdot}nH_2O$ (n = 1, 2, 4) were performed using the programs *DASH* (David *et al.*, 1998) and *DICVOL*91 (Boultif & Louër, 1991) and led to lattice para-

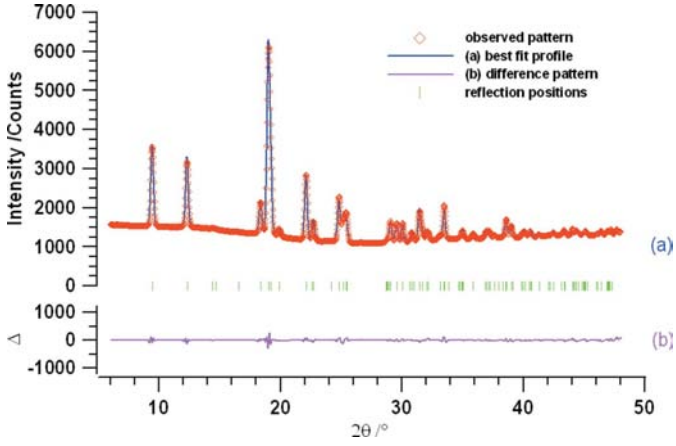

Figure 6
Scattered X-ray intensity for $MgCl_2{\cdot}2H_2O$ at T = 369 K as a function of diffraction angle 2θ. Shown are the observed pattern (diamonds), the best Rietveld-fit profile in °2θ (*a*), the difference curve between observed and calculated profile (*b*), and the reflection markers (vertical bars). The wavelength was λ = 0.92187 Å. The R values are R_p = 0.0010, R_{wp} = 0.017, and R_{F^2} = 0.072.

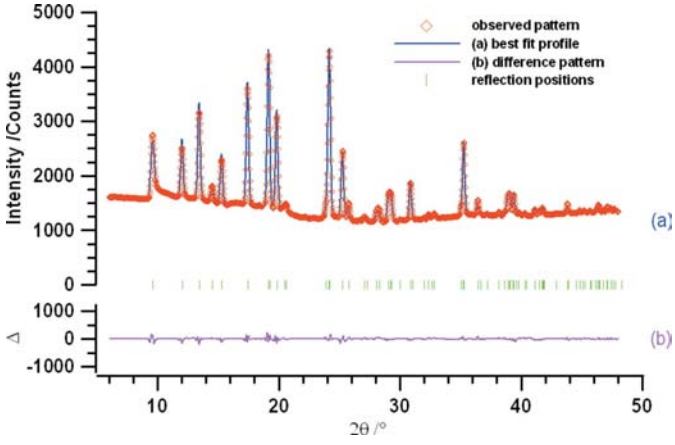

Figure 5
Scattered X-ray intensity for $MgCl_2{\cdot}4H_2O$ at T = 358 K as a function of diffraction angle 2θ. Shown are the observed pattern (diamonds), the best Rietveld-fit profile in °2θ (*a*), the difference curve between observed and calculated profile (*b*), and the reflection markers (vertical bars). The wavelength was λ = 0.92187 Å. The R values are R_p = 0.0114, R_{wp} = 0.019, and R_{F^2} = 0.078.

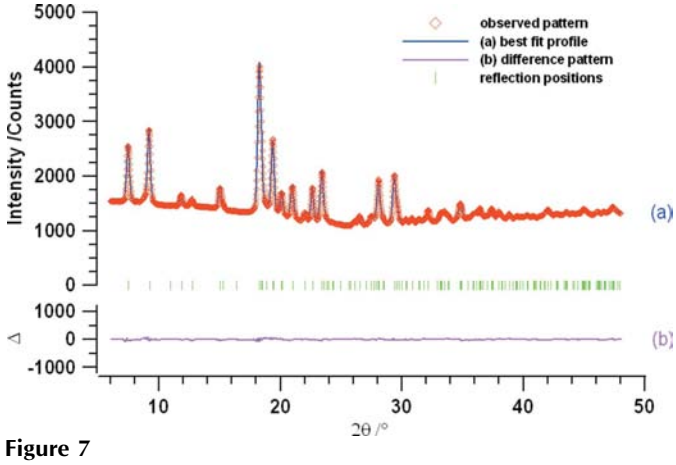

Figure 7
Scattered X-ray intensity for $MgCl_2{\cdot}H_2O$ at T = 434 K as a function of the diffraction angle 2θ. Shown are the observed pattern (diamonds), the best Rietveld-fit profile in °2θ (*a*), the difference curve between observed and calculated profile (*b*), and the reflection markers (vertical bars). The wavelength was λ = 0.92187 Å. The R values are R_p = 0.0091, R_{wp} = 0.012, and R_{F^2} = 0.075.

meters given in Table 1. The possible space groups (*C*2*cm*, *Cmc*2_1 and *Cmcm* for $MgCl_2{\cdot}4H_2O$, C2, *Cm* and *C*2/*m* for $MgCl_2{\cdot}2H_2O$, and *Pn*2_1*a* and *Pnma* for $MgCl_2{\cdot}H_2O$) and the number of formula units per unit cell ($Z = 2$) were found by applying the extinction rules and volume increments.

A preliminary Le Bail fit (LeBail *et al.*, 1988) using the program *GSAS* (Larson & Von Dreele, 2000) worked well after fixing the lattice parameters. For the description of the peak profile, a pseudo-Voigt function (Thompson *et al.*, 1987) was used. Structural starting models of $MgCl_2{\cdot}nH_2O$ (n = 1, 2, 4) for Rietveld refinement were subsequently found with the Monte Carlo simulated annealing program *FOX* (Favre-Nicolin & Cerný, 2002) using the lattice parameters from the previous Le Bail fit in space groups *Cmcm* (scan No. 63) for $MgCl_2{\cdot}4H_2O$, *C*2/*m* (scan No. 12) for $MgCl_2{\cdot}2H_2O$ and *Pnma* (scan No. 62) for $MgCl_2{\cdot}H_2O$. The angular range was restricted from 6.0 to 42.83° (2θ) ($\sin\theta/\lambda = 0.4$). The profile parameters needed for the *FOX* program were taken from the profile matching of the first peaks of $MgCl_2{\cdot}nH_2O$ (n = 1, 2, 4) using the program *FULLPROF* (Rodriguez-Carvajal, 1990). Initially, an ideal $MgCl_2O_4$ octahedron was created in *FOX*, with two Cl atoms occupying the vertices and four O atoms occupying the equatorial positions. H atoms were neglected. In all cases, after approximately 1 million cycles (corresponding to 1 h on a 2 GHz standard PC) promising starting models in terms of crystal packing were found and subjected to Rietveld refinement using the *GSAS* program. Starting values for the lattice parameters, the background, and the peak profile were taken from the corresponding Le Bail fits. In the case of $MgCl_2{\cdot}nH_2O$ (n = 1, 2), H atoms were introduced and held fixed at idealized positions. This was not possible for $MgCl_2{\cdot}4H_2O$ owing to the apparent disorder in the crystal structure. All other non-H atoms (Mg, Cl and O) were freely refined using isotropic displacement parameters. Quick convergence was reached for all three crystal structures. Nevertheless, in the case of $MgCl_2{\cdot}4H_2O$, the bond lengths of Mg—O and Mg—Cl were out of the expected ranges with a large displacement parameter of Mg. An anisotropic refinement of the displacement parameters of the O and Cl atoms located on the special site 4(*c*) (*m*2*m* symmetry; 0, *y*, 1/4) showed a spread along the *c* axis. Therefore, the symmetry restrictions for these O and Cl atoms were lowered from the position 4(*c*) to 8(*f*) (*m* symmetry; 0, *y*, *z*) with a site occupancy of 50%, introducing positional disorder. A subsequent Rietveld refinement immediately converged and led to reasonable bond lengths and displacement parameters, thus confirming the modified structural model.

The maximum residuals in the electron density map found were between −0.51 and 0.43 e Å^{-3} for $MgCl_2{\cdot}4H_2O$, between −0.38 and 0.41 e Å^{-3} for $MgCl_2{\cdot}2H_2O$, and between −0.54 and 0.55 e Å^{-3} for $MgCl_2{\cdot}H_2O$. The final Rietveld plots are given in Figs. 5–7. Crystallographic data and agreement factors of the Rietveld refinement are listed in Table 1. Atomic coordinates, bond lengths and bond angles are presented in the supplemental material.[1]

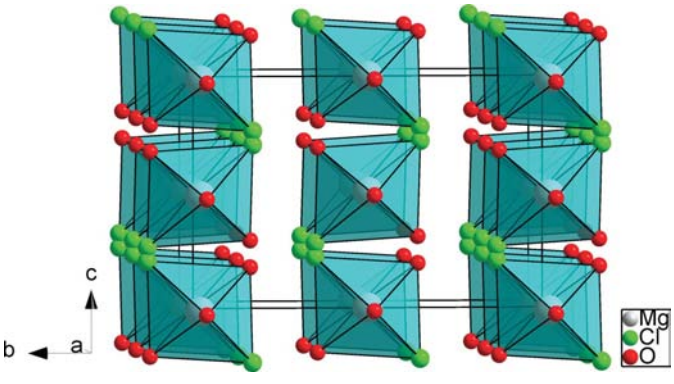

Figure 8
Crystal packing of $MgCl_2{\cdot}4H_2O$ in a parallel projection approximately down the crystallographic *a* axis. Mg-atom positions are in white, Cl-atom positions are in green and O-atom positions are in red. Semi-transparent $MgCl_2(H_2O)_4$ polyhedra are drawn. Note that the occupancy of each $MgCl_2(H_2O)_4$ octahedron is 50%.

4. Structure description

4.1. Crystal structure of $MgCl_2{\cdot}4H_2O$

The crystal packing of $MgCl_2{\cdot}4H_2O$ is shown in Fig. 8 in a projection down the *a* axis. The disordered crystal structure of $MgCl_2{\cdot}4H_2O$ consists of discrete $Mg(H_2O)_4Cl_2$ octahedra with the two Cl atoms occupying the axial positions and the four water molecules occupying the equatorial positions. The Mg—Cl bond lengths of 2.311 Å and Mg—O bond lengths of 2.108 and 2.109 Å are within the expected ranges. The deviations of the bond angles from ideal octahedral geometry is below 5°.

Owing to the disorder, only every second $Mg(H_2O)_4Cl_2$ octahedron is occupied, leading to a shortest intermolecular distance of 3.104 Å for Cl···O2, enabling the formation of hydrogen bonds between neighboring octahedra.

The crystal structure of $MgCl_2{\cdot}4H_2O$ (PDF-53-258) as reported by Kaduk (2002) in space group $P2_1/c$ exhibits discrete $Mg(H_2O)_4Cl_2$ octahedra and can be considered an ordered variant of our findings.

4.2. Crystal structures of $MgCl_2{\cdot}2H_2O$ and $MgCl_2{\cdot}H_2O$

The crystal structure of $MgCl_2{\cdot}2H_2O$ can be described as a one-dimensional chain structure consisting of edge-sharing $Mg(H_2O)_2Cl_4$ octahedra parallel to the *c* axis (Fig. 9). The Cl atoms occupy the four bridging equatorial positions and the water molecules are located at axial positions.

The crystal structure of $MgCl_2{\cdot}H_2O$ consists of one-dimensional double chains of edge-sharing $Mg(H_2O)Cl_5$ octahedra parallel to the *b* axis (Fig. 10). The Cl atoms act as bridging ligands, occupying the four equatorial and one of the axial positions. Thus, three edges of each octahedron are shared, two perpendicular to the chain axis and one connecting the two neighboring single chains. The water molecule is located at the second axial position which is unbridged.

[1] Supplementary data for this paper are available from the IUCr electronic archives (Reference: KD5011). Services for accessing these data are described at the back of the journal.

The quality of the crystal structure descriptions of $MgCl_2{\cdot}2H_2O$ and $MgCl_2{\cdot}H_2O$ (Kaduk, 2002)[2] has been considerably improved by using synchrotron powder diffraction data on single phases.

4.3. Crystal structure of $MgOHCl{\cdot}nH_2O$ ($0 \leq n \leq 1.0$)

The powder pattern of the phases (*e*) and (*f*) which are attributed to $MgOHCl{\cdot}nH_2O$ ($0 \leq n \leq 1.0$) reflect the low crystallinity of the material and cannot be unambiguously indexed, thus preventing the determination of their crystal structure. Nevertheless, a visual comparison of the powder patterns of phases (*e*) at $T = 542$ K and (*f*) at $T = 640$ K with the simulated powder pattern of $MgCl_2$ using the data of Partin & O'Keeffe (1991) clearly reveals many similarities between the peak positions and intensities (Fig. 5). Additional reflections indicate a distortion to a lower symmetric unit cell. Nevertheless, it may thus be speculated that the basic crystal structures are identical. From TGA analysis of bischofite (Fig. 2) it is known that water and hydrogen chloride are continuously removed from the crystal structure in the phase range of $MgOHCl{\cdot}nH_2O$ ($0 \leq n \leq 1.0$). The peak shape, which is typical for the presence of stacking faults, suggests severe disorder of a layer-type crystal structure of phases (*e*) and (*f*).

Chloromagnesite, $MgCl_2$, crystallizes in the space group $R\bar{3}m$ and is isostructural to $CdCl_2$, which is considered to be the aristotype for all water-free divalent metal chlorides $A^{2+}2(Cl^-)$ (A = Ca, Mn, Fe, Co, Ni, Cu, Mg). In this structure type, the chlorine atoms are forming a distorted cubic closed packing (c.c.p.) with the metal atoms occupying one quarter of the octahedral voids, thus forming two-dimensional sheets of edge-sharing ACl_6 octahedra (Partin & O'Keeffe, 1991). Replacing half of the chlorine anions by hydroxyl groups leads to the known structure type $A^{2+}(OH^-)(Cl^-)$ for *e.g.* A = Ca, Cu, Cd, Mg with edge-sharing $A(OH)_3Cl_3$ octahedra. Despite the almost identical packing compared with the divalent metal chlorides, a variety of space groups for metal hydroxyl chlorides $A^{2+}(OH^-)(Cl^-)$ is realised depending on the different degrees of distortions owing to the size and polarizability of the cation. Additional non-bonded water molecules can intercept these layers while preserving the basic crystal structure.

5. Discussion and conclusion

While comparing different publications on the dehydration process of bischofite (*e.g.* Kashani-Nejad *et al.*, 2005; Galwey & Laverty, 1989; Kirsh *et al.*, 1987; Gardner & Messing, 1984; Herbstein *et al.*, 1982; Petzold & Naumann, 1980; Buzagh-Gere *et al.*, 1973), it is obvious that the transition temperatures of the various decomposition phases as derived from DTA, TGA and DTG analyses are strongly dependent on the experimental conditions. Our results on thermogravimetric analysis (TGA) and mass spectrometry for mass numbers 18 (H_2O) and 36 (HCl) of bischofite are shown in Fig. 2. The weight loss of bischofite is estimated at 17.7% for $MgCl_2{\cdot}4H_2O$, 35.4% for $MgCl_2{\cdot}2H_2O$, 44.3% for $MgCl_2{\cdot}H_2O$, 53.4% for $MgOHCl{\cdot}H_2O$, 59.6% for $MgOHCl{\cdot}0.3H_2O$, 62.2% for MgOHCl, and 66.7% for $MgCl_2$ and MgO, as indicated in Fig. 2.

All the previously reported phase transitions could be confirmed by *in situ* synchrotron powder diffraction data as a function of temperature (Fig. 3) in the range $298 \leq T \leq 873$ K. Based on these diffraction data, a reaction scheme for the

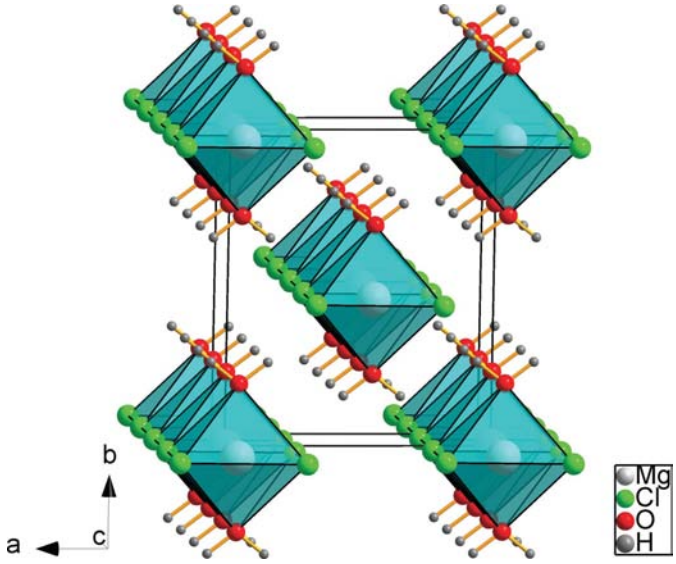

Figure 9
The crystal packing of $MgCl_2{\cdot}2H_2O$ in a parallel projection approximately down the crystallographic *c* axis. Mg-atom positions are in white, Cl-atom positions are in green, O-atom positions are in red and H-atom position are in gray. Semi-transparent $MgCl_2(H_2O)_4$ polyhedra are drawn.

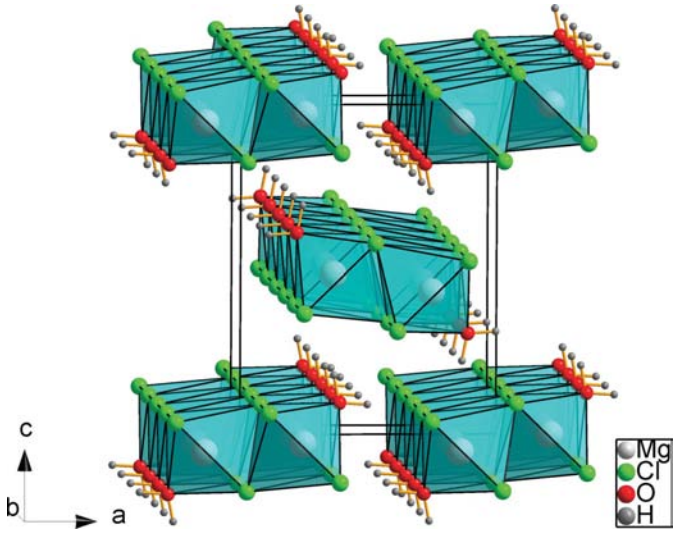

Figure 10
The crystal packing of $MgCl_2{\cdot}H_2O$ in a parallel projection approximately down the crystallographic *b* axis. Mg-atom positions are in white, Cl-atom positions are in green, O-atom positions are in red and H-atom position are in gray. Semi-transparent $MgCl_2(H_2O)_4$ polyhedra are drawn.

[2] Atomic coordinates are given in the comment section of PDF 53-259 and PDF 53-260.

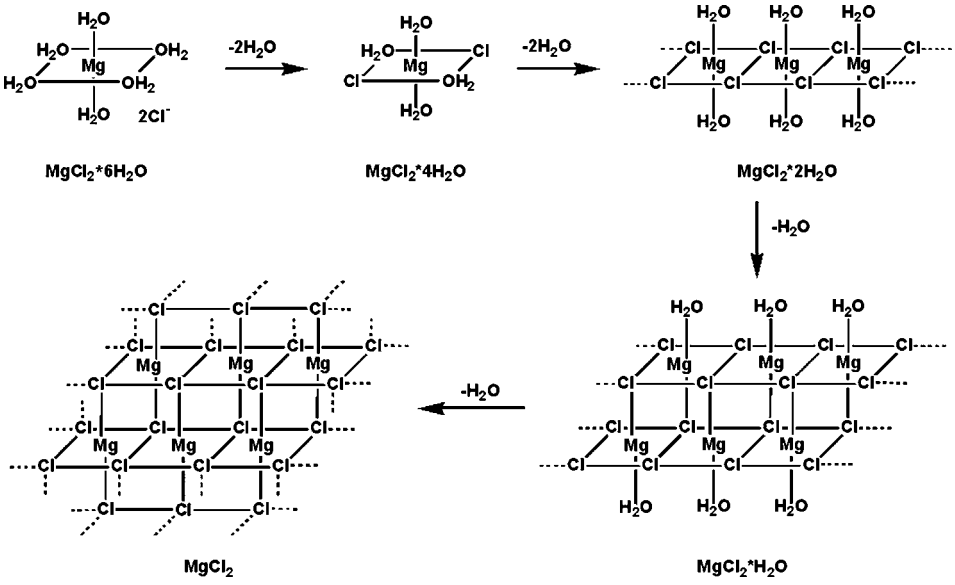

Figure 11
Changes in the packing scheme upon dehydration of bischofite.

thermal decomposition of bischofite including transition temperatures has been prepared (Table 2). Compared with the TGA data, the transition temperatures are shifted towards lower temperatures which can be explained by the different humidity conditions and the different nature of the gases used for purging.

The structural changes during the thermal decomposition from $MgCl_2{\cdot}6H_2O$ to anhydrous $MgCl_2$ are summarized in Fig. 11, revealing a clear trend in the coordination of the Mg atoms. It is obvious that O atoms are the preferred ligands compared with Cl atoms. The following packing arrangements are found depending on the decreasing amount of crystal water. The crystal structure of bischofite consists of isolated and ordered $Mg(H_2O)_6^{2+}$ octahedra and Cl^- anions (Fig. 1). After the loss of two water molecules, the crystal structure of $MgCl_2{\cdot}4H_2O$ consists of isolated and disordered but neutral $Mg(H_2O)_4Cl_2$ octahedra with the two Cl anions in *trans*-equatorial positions. Upon the release of the next two water molecules, the crystal structure of $MgCl_2{\cdot}2H_2O$ is forced to form infinite single chains consisting of $Mg(H_2O)_2Cl_4$ octahedra with the Cl atoms occupying all the equatorial positions. The next loss of a single water molecule results in the building of infinite double chains of $Mg(H_2O)Cl_5$ octahedra in the crystal structure of $MgCl_2{\cdot}H_2O$ where the remaining water molecule occupies the axial position pointing away from the chain. After stripping the last remaining water molecule, the well known infinite sheet structure of $MgCl_2$ is formed. The occurrence of two distinct magnesium hydroxychloride phases $MgOHCl{\cdot}nH_2O$ ($0 \leq n \leq 1.0$) which occur before anhydrous $MgCl_2$ is formed has been confirmed (Figs. 3 and 4). The poor crystallinity so far prevented the direct determination of their crystal structures, but due to the apparent similarity to the powder pattern of $MgCl_2$ it may be concluded that their crystal structure is a distorted variant of the $MgCl_2$ structure with sheets of $MgCl_3(OH)_3$ octahedra and free water molecules between the sheets.

This work was carried out in part at the National Synchrotron Light Source at Brookhaven National Laboratory, which is supported by the US Department of Energy, Division of Materials Sciences and Division of Chemical Sciences under contract DE-AC02-98CH10886 by the US Department of Energy, Division of Chemical Sciences, Office of Basic and Energy Sciences. Special thanks go to Dr Andreas Leineweber (Max Planck Institute for Metals Research) for helpful discussion and Dr Christian P. M. Oberndorfer (Max Planck Institute for Solid State Research) for conducting the DTA/TGA/MS as well as the DSC measurements. Financial support by the Bundesministerium für Bildung und Forschung (BMBF), the Rigaku Corporation, and the Fonds der Chemischen Industrie (FCI) is gratefully acknowledged.

References

Agron, P. A. & Busing, W. R. (1985). *Acta Cryst.* C**41**, 8–10.
Andress, K. R. & Gundermann, J. (1934). *Z. Kristallogr.* **87**, 345–369.
Boultif, A. & Louër D. (1991). *J. Appl. Cryst.* **24**, 987–993.
Brandenburg, K. & Putz, H. (2006). *MATCH*, Version 1.4b. Crystal Impact GbR, Bonn, Germany.
Buzagh-Gere, E., Gal, S. & Simon, J. (1973). *Z. Anorg. Allg. Chem.* **400**, 37–44.
Chizmeshya, A. V. G., McKelvy, M. J., Sharma, R., Carpenter, R. W. & Bearat, H. (2002). *Mater. Chem. Phys.* **77**, 416–425.
Chupas, P. J., Circaolo, M. F., Hanson, J. C. & Grey, C. P. (2001). *J. Am. Chem. Soc.* **123**, 1694–1702.
David, W. I. F., Shankland, K. & Shankland, N. (1998). *Chem. Commun.* pp. 931–932.
Favre-Nicolin, V. & Cerný, R. (2002). *J. Appl. Cryst.* **35**, 734–743.
Galwey, A. K. & Laverty, G. M. (1989). *Thermochim. Acta*, **138**, 115–127.
Gardner, T. J. & Messing, G. L. (1984). *Thermochim. Acta*, **78**, 17–27.
Herbstein, F. H., Kapon, M. & Weissman, A. (1982). *Isr. J. Chem.* **22**, 207–213.
Hinrichsen, B., Dinnebier, R. E. & Jansen, M. (2006). *Z. Kristallogr.* Suppl. **23**, 231–236.
Kaduk, J. A. (2002). *Acta Cryst.* B**58**, 370–379.
Kashani-Nejad, S., Ng, K. W. & Harris, R. (2005). *Metall. Trans. B*, **36**, 153–157.
Kirsh, Y., Yariv, S. & Shoval, S. (1987). *J. Thermal Anal.* **32**, 393–408.
Larson, A. C. & Von Dreele, R. B. (2000). *GSAS.* Report LAUR 86–748. Los Alamos National Laboratory, New Mexico, USA.

Le Bail, A., Duroy, H. & Fourquet, J. L. (1988). *Mater. Res. Bull.* **23**, 447–452.
Parise, J. B., Cahill, C. L. & Lee, Y. J. (2000). *Can. Mineral.* **38**, 777–800.
Partin, D. E. & O'Keeffe, M. (1991). *J. Solid State Chem.* **95**, 176–183.
Petzold, D. & Naumann, R. (1980). *J. Thermal Anal.* **19**, 25–34.
Rodriguez-Carvajal, J. (1990). Abstracts of the Satellite Meeting on Powder Diffraction of the XV Congress of the IUCr, p. 127. Toulouse, France.
Sugimoto, K., Dinnebier, R. E. & Schlecht, T. (2006). *J. Appl. Cryst.* **39**, 739–744.
Thompson, P., Cox, D. E. & Hastings, J. B. (1987). *J. Appl. Cryst.* **20**, 79–83.